Draft version February 5, 2008
Preprint typeset using LaTeX style emulateapj v. 6/22/04

THE DIVERSE INFRARED PROPERTIES OF A COMPLETE SAMPLE OF STAR-FORMING DWARF GALAXIES

Jessica L. Rosenberg*, Matthew L. N. Ashby
Harvard-Smithsonian Center for Astrophysics, 60 Garden Street MS 65, Cambridge, MA 02138

John J. Salzer
Wesleyan University, Department of Astronomy, Middletown, CT 06459

Jia-Sheng Huang
Harvard-Smithsonian Center for Astrophysics, 60 Garden Street MS 65, Cambridge, MA 02138
Draft version February 5, 2008

ABSTRACT

We present mid-infrared Spitzer Space Telescope observations of a complete sample of star-forming dwarf galaxies selected from the KPNO International Spectroscopic Survey. The galaxies span a wide range in mid-infrared properties. Contrary to expectations, some of the galaxies emit strongly at 8 μm indicating the presence of hot dust and/or PAHs. The ratio of this mid-infrared dust emission to the stellar emission is compared with the galaxies' luminosity, star-formation rate, metallicity, and optical reddening. We find that the strength of the 8.0μm dust emission to the stellar emission ratio is more strongly correlated with the star-formation rate than it is with the metallicity or the optical reddening in these systems. Nonetheless, there is a correlation between the 8.0 μm luminosity and metallicity. The slope of this luminosity-metallicity correlation is shallower than corresponding ones in the B-band and 3.6 μm. The precise nature of the 8.0μm emission seen in these galaxies (i.e., PAH versus hot dust or some combination of the two) will require future study, including deep mid-IR spectroscopy.

Subject headings: galaxies:dwarf, galaxies:starburst, infrared:galaxies, galaxies:abundances, dust, extinction

1. INTRODUCTION

Low-mass, low-metallicity systems are the building blocks in hierarchical galaxy formation scenarios. Star-formation processes in these systems may play a critical role in the evolution of galaxies including the feedback of metals into the intergalactic medium (Mac Low and Ferrara 1999; Ferrara and Tolstoy 2000; Silich and Tenorio-Tagle 2001), the suppression of low-mass halos that are over-produced in semi-analytic models of galaxy formation (Kravtsov et al. 2004), and the color evolution of galaxies. Nearby actively star-forming dwarf galaxies are possible analogs to these high redshift systems. These galaxies are gas-rich, metal poor, and undergoing bursts of star formation in the local universe. As low-redshift systems, these galaxies can be studied in much greater detail than is possible for galaxies in the high redshift universe.

At visible wavelengths dwarf star-forming galaxies are very blue and exhibit strong nebular emission lines. Many of the systems are very compact with morphologies like large HII regions, although some do resemble dwarf irregular or dwarf spiral galaxies. At longer wavelengths dust emission from reprocessed starlight is a good tracer of star formation in galaxies (Dwek et al. 1998). However, observations of a sample of emission-line galaxies with the Infrared Astronomical Satellite (IRAS) have indicated that dwarf star-forming galaxies are less likely to be detected in the far infrared than their higher luminosity counterparts (Salzer & MacAlpine 1988). These galaxies could be more difficult to detect in the FIR due to a lack of dust, a different dust grain size distribution, or a different dust temperature distribution. The mid-infrared to millimeter spectral energy distributions (SEDs) of a small number of nearby dwarf galaxies selected for their high star-formation rates indicate that some dwarf star-forming systems do contain a significant amount of dust but that the systems probably lack PAHs and have a small average dust grain size (Galliano et al. 2005, 2003).

The launch of the Spitzer Space Telescope (Werner et al. 2004) has opened up a new window on the study of star-formation processes in galaxies. The IRAC instrument (Fazio et al. 2004) in particular allows us to measure both the stellar emission and the hot dust and PAH emission in local galaxies. One of the first dwarf galaxies to be examined in detail with Spitzer was the blue compact dwarf galaxy SBS 0335-052 (Houck et al. 2004). This galaxy, with one of the lowest known metallicities ($Z \approx Z_{\odot}/20$, Izotov et al. 1997), is known to have dust but it lacks PAH emission (Thuan et al. 1999; Plante and Sauvage 2002). The mid-infrared flux from the galaxy is dominated by a cold dusty envelope ($\sim$65 K) and shows evidence for a warm dust component ($\sim$150 K). While SBS 0335-052 is an unusual system, Hogg et al. (2005) examined the mid-infrared colors of $\sim$10 low luminosity galaxies and Engelbracht et al. (2005) examined a sample of low

*National Science Foundation Astronomy and Astrophysics Postdoctoral Fellow
Electronic address: jlrosenberg@cfa.harvard.edu

metallicity galaxies with Spitzer and both concluded that a significant fraction of the low-luminosity and low-metallicity systems show a deficit of PAH emission. In the case of the Hogg et al. (2005) data, there are no spectra to discern the difference between PAHs and a hot dust continuum but Engelbracht et al. (2005) do have spectra and draw the same conclusion – the mid-infrared shows a PAH deficit but an 8.0 μm excess consistent with hot dust emission.

Overall, only a small sample of dwarf galaxies has been looked at with Spitzer to date. We present the first detailed look at a statistically complete sample of dwarf galaxies known to be undergoing a burst of star formation. In §2 we discuss the selection of this sample, the optical and infrared observations and the data reduction. In §3 we present the observational results for the sample from the optical, near infrared, and mid-infrared data and then we discuss those results in §4.

2. SAMPLE SELECTION, OBSERVATIONS, AND DATA REDUCTION

2.1. *KISS Observations*

The KPNO International Spectroscopic Survey (KISS) is a modern objective-prism survey that combines the methodology of many of the classic wide-field color- and line-selected surveys (e.g., Markarian 1967; Smith et al. 1976; MacAlpine et al. 1977; Wasilewski 1983; Zamorano et al. 1994) with the higher sensitivity of a CCD detector. The survey method is described in detail by Salzer et al. (2000). KISS selects objects for inclusion in the survey lists if they possess a strong ($> 5\sigma$) emission line in their low-dispersion objective-prism spectra. The survey has been carried out in two distinct spectral regions: the blue portion (4800 – 5500 Å) where the primary line observed is [O III]λ5007, and the red region (6400 – 7200 Å) where galaxies are selected by their Hα emission. To date, the survey has produced one list of emission-line galaxy (ELG) candidates in the blue (Salzer et al. 2002) and three in the red (Salzer et al. 2001; Gronwall et al. 2004; Jangren et al. 2005, hereafter KR3). For the current study, we have selected a sample of dwarf star-forming galaxies from KR3. This survey list was derived from objective-prism data taken of the NOAO Deep Wide-Field Survey (NDWFS) area located in Boötes. Both of the NDWFS fields were targeted by KISS to take advantage of the tremendous amount of multi-wavelength data planned for these areas.

All of the KISS ELG candidates in the Boötes field possess follow-up slit spectra (Salzer et al. 2005a). Higher dispersion follow-up spectra are necessary in order to verify the reality of the putative emission lines seen in the objective-prism spectra. In addition, the survey data alone do not have sufficient dispersion or spectral range to provide accurate redshifts or to distinguish between the various activity types that might be present in a line-selected sample (e.g., star-forming galaxies vs. AGNs). These follow-up spectra provide us with a great deal of useful information (e.g., accurate redshifts, emission-line fluxes and line ratios, reddening and metallicity estimates). The combination of the accurate B and V photometry from the original survey lists with these follow-up spectra allow for the construction of a fairly complete picture of the properties of the KISS ELGs.

The selection of the KISS galaxies from the KR3 list was defined by several criteria. For emission-line galaxies selected by their Hα emission (in the red), the redshift limit of the survey is $z = 0.095$. The two selection criteria used to define the sample were that the galaxies exhibit spectra consistent with excitation by star-formation processes (i.e., AGNs were excluded), and that they have a B-band absolute magnitude $M_B > -18.0$ (for $H_0 = 75$ km s^{-1} Mpc^{-1}). Thus these galaxies are selected to be star-forming dwarf galaxies. These criteria produced a list of 26 galaxies within the NDWFS Boötes area. However, of those 26 galaxies, only 19 overlap with the Spitzer Shallow Survey area because the Spitzer survey field is smaller than the NDWFS field. We discuss only these 19 galaxies in our analysis. Table 1 presents the KISS data for this sample.

All magnitudes discussed in this paper are Vega relative magnitudes.

2.2. *2MASS and NOAO Deep Wide-Field Survey Data*

The field from which our sample of 19 dwarf star-forming galaxies was drawn has multi-wavelength optical and infrared coverage from the NDWFS (Jannuzi and Dey 1999; Jannuzi 2005; Dey 2005) and the 2 Micron All-Sky Survey (2MASS). The NDWFS provides B, R, and I-band data that complement the broad-band B and V band optical data from the KISS survey. K-band data from the NDWFS are also available for 11 of the 19 galaxies in the field. The K-band for the remaining galaxies are not yet publicly available from the NDWFS.

The 2MASS data have been included in this table for completeness and as a reference for future work with this sample even though we do not use the data here. The 2MASS data are only deep enough to detect four galaxies in this sample. Because these four sources are compact and near the 2MASS detection limits, they are only identified in the point source catalog. The photometry available from the NDWFS is more reliable than the 2MASS data. Note that for the 2 sources for which 2MASS and NDWFS data exist, the NDWFS measurements are much brighter. The 2MASS point source measurements are missing a lot of the extended galaxy flux that is below the detection limit of the survey.

The agreement between the KISS and NDWFS B-band photometry is excellent for all of the galaxies except KISS 2344. This object is very extended and was not well fit by the automated NDWFS software (SExtractor "auto" magnitudes are used, Bertin and Arnouts 1996), which underestimated the flux of this source by a magnitude relative to the KISS value. For the rest of the sample, however, the average difference between the KISS and NDWFS magnitudes for the rest of the sample is only 0.04 magnitudes. Table 2 contains the NDWFS and 2MASS photometry for the 19 galaxies in the sample.

2.3. *Spitzer Observations*

Using the Infrared Array Camera (IRAC) aboard the Spitzer Space Telescope, the majority of the NDWFS was mapped at 3.6 - 8.0 μm in January 2004 (Eisenhardt et al. 2004). This project, known as the IRAC Shallow Survey, covered 8.5 square degrees – most but not all of the NDWFS field. The observed region was selected to have the lowest background in the IRAC bands. Because not all of the NDWFS field is covered,

FIG. 1.— Three color composite images at 3.6, 4.5, and 8.0 μm (blue, green, and red respectively). These images have not been point-source subtracted. Redshifts are indicated for all objects. JPEG file of figure is included with the download.

three of the 26 KISS galaxies in this field are just off the eastern edge of the field and four are in the southeast corner of the field where there is a hole in the coverage. For the remainder of the paper we discuss only the 19 sources with coverage in the Spitzer IRAC bands. Each position in the survey field was covered with three 30 s IRAC frames, resulting in a depth of 19.1, 18.3, 15.9, and 15.2 Vega magnitudes (5σ) at 3.6, 4.5, 5.8, and 8.0μm, respectively. This depth was reached by tiling the $5' \times 5'$ IRAC FOV over the field.

The basic image processing and mosaicing of the Spitzer data are discussed in detail by Eisenhardt et al. (2004). From the resulting mosaiced images (Version 1.1), postage stamps 100 × 100 pixels in size were extracted for our sample galaxies (except for KISS 2344 which is more extended so we extracted a 200 × 200 pixel postage stamp, the pixel scale for all postage stamps is $0.86''$ per pixel).

Figure 1 shows three color images for all of the galaxies in the sample. The images, created prior to the point source subtraction, provide a look at the colors and morphologies of the objects in the sample.

Because of the high point source density in the fields, we subtracted point sources from the 3.6 and 4.5 μm data prior to deriving photometry for the galaxies. In the 3.6 μm band 7 – 39% of the flux in the aperture is due to the point sources in the vicinity of our galaxy. The flux due to point sources in the 4.5 μm band is less than in the 3.6 μm band for most sources, but the range is from $\sim$3 – 36%. The point source removal was done using the APEX program within the MOPEX package provided by the Spitzer Science Center. The PSF used was constructed by Marengo et al. (2005) and was smoothed to match the resolution of the mosaiced images and then used by the APEX program to identify candidate point sources in the images. We defined the APEX detection parameters so that all of the stars were selected, but the result was that non-stellar peaks in faint parts of the galaxy were also identified. The point sources selected by APEX were then checked by hand in order to eliminate non-stellar sources from the point source list. The resulting point sources were then subtracted from the 3.6 and 4.5 μm images. Overall the point source subtraction worked well, but the centers of the brightest stars which are non-linear or saturated left a residual. For the 5.8 and 8.0 μm data, the point source density was not high enough to warrant point source subtraction as was done in the shorter wavelength bands.

Galaxy photometry was performed on the processed, mosaiced, and, for the 3.6 and 4.5 μm images, point source-subtracted images using the ELLIPSE routine within IRAF. Point sources in the 5.8 and 8.0 μm bands and post point source subtraction residuals in the 3.6 and 4.5 μm bands were masked using ELLIPSE. An elliptical aperture was fit to the galaxy, the aperture ellipticity and position angle were fixed, and then apertures were computed over the background region beyond the extent of the galaxy. The level determined from the background annulus was then used to subtract the local background from the image. After the subtraction, the fitting was rerun using these same aperture parameters out to the largest radius before the background was reached as determined from the curve of growth of the flux. The aperture defined by the 3.6 μm data was then used to determine the flux in the other bands. The results of the IRAC photometry are presented in Table 3.

3. RESULTS

The combination of the optical and IRAC observations provide a probe of stellar and dust emission in galaxies in the local universe. Figure 2 shows a template SED for an irregular galaxy. This SED template is based on the Coleman et al. (1980) distribution derived in the optical and the Lu et al. (2003) distribution in the infrared. The template is an empirical derivation of the SED extrapolated between the available bands. The optical bands, as well as the 3.6 and 4.5 μm IRAC bands probe the stellar emission from the galaxy. The 3.6 and 4.5 μm bands, while dominated by the stellar emission, can also be influenced by hot dust emission (particularly the 4.5 μm band; Roussel et al. 2005). The 5.8 and 8.0 μm IRAC bands probe the Rayleigh-Jeans tail of the hot dust continuum as well as the PAH emission features from the galaxy. There is a degeneracy between the slope of the hot dust continuum and the strength of the PAH emission features which does not allow us to distinguish between them using broad-band color information. For this analysis we focus on the 3.6 μm and the 8.0 μm emission as probes of the stellar and PAH or hot dust emission in the galaxies that we are studying. The [3.6] − [8.0] color provides a measure of the dust-to-stars ratio in the galaxies.

The points in Figure 2 show SEDs for two of the galaxies in this sample to illustrate the differences in their properties. The circles show the SED for KISS 2309 while the triangles show the SED for KISS 2349. The two SEDs have been normalized so that they overlap in the K-band. The optical/near-infrared photometry has been computed in different apertures for the KISS and NDWFS data, but the extremely good correlation between the magnitudes measured in the B-band ($\sigma = 0.04$) indicates that the values are consistent. A fixed aperture is used for all of the mid-infrared measurements, but this are not the same aperture as used in the optical/near-infrared. Because we use a large aperture intended to contain all of the light, the aperture corrections between the mid-infrared and the optical/near-infrared should be small. The application of an aperture correction would result in a small vertical shift for all of the mid-infrared points in Figure 2.

Figure 2 illustrates the relationship between the mid-infrared colors of two sample galaxies and the general shapes of their SEDs. We leave a discussion of the detailed SED fitting to a forthcoming paper. The KISS 2349 SED has a very red [3.6] − [8.0] color ([3.6] − [8.0] = 2.92). This SED clearly shows evidence for hot dust or, possibly, PAH emission. By contrast, the SED of KISS 2309 continues to fall into the mid-infrared showing much less hot dust or PAH emission ([3.6] − [8.0]

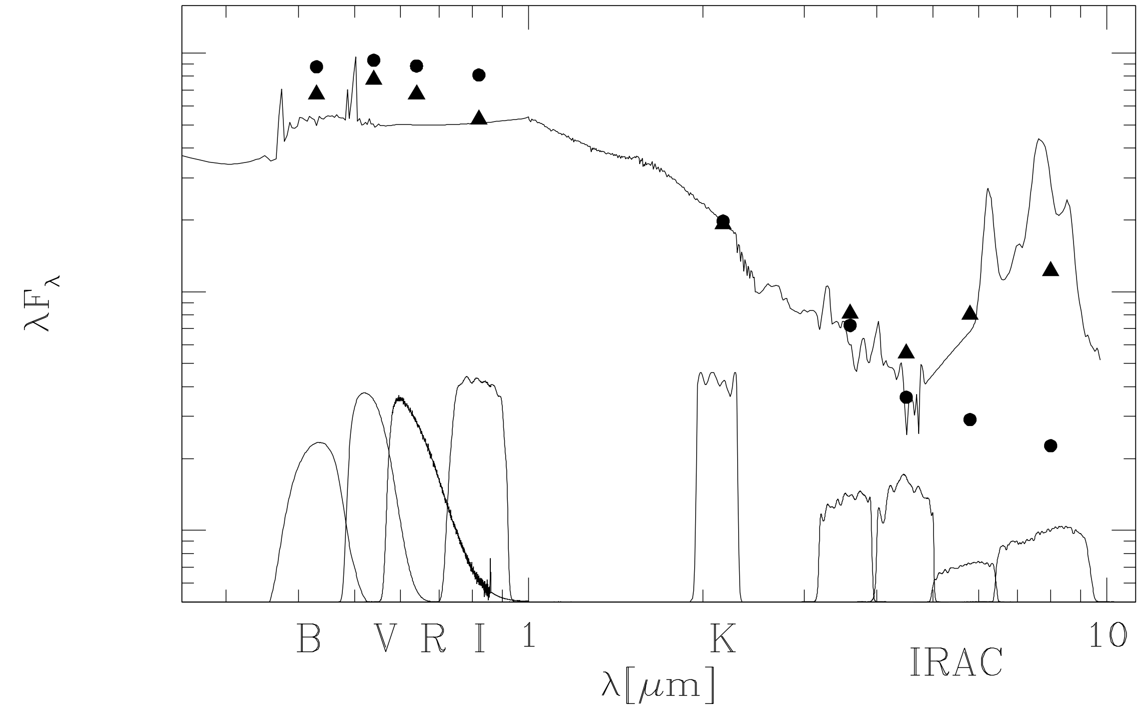

FIG. 2.— An empirical irregular galaxy spectral template showing stellar emission at short wavelengths and the dust-emission in the mid-infrared. The template is based on the Coleman et al. (1980) SED in the optical and the Lu et al. (2003) SED in the infrared. The IRAC filter sensitivities as well as B, V, R, I, and K-band filter response functions are shown (B and V are Schmidt filters while R and I are Mosaic filters from http://www.noao.edu/kpno/filters/filters.html. The K-band data are from http://www.noao.edu/kpno/manuals/onis/mopopulation.html and the IRAC data are from http://ssc.spitzer.caltech.edu/documents/som/.) The points show the SEDs for KISS 2309 (circles) and KISS 2349 (triangles). These galaxy SEDs have been scaled to the same value in the K-band for comparison. These SEDs illustrate the range of mid-infrared colors observed in this sample.

= 1.21), but the colors are still in excess of the extrapolation of the stellar portion of the template. All of the galaxies in this sample show evidence for 8.0 μm emission in excess of the stellar light. Both galaxies show extremely blue optical colors even relative to the K-band flux. These galaxies are dominated by a young stellar population even relative to an average irregular galaxy.

3.1. *Properties of the Sample*

Despite the low detection rate for star-forming dwarf galaxies at longer infrared wavelengths (Salzer & MacAlpine 1988), we detected all 19 galaxies in all four bands with only a short exposure time. Only at 5.8 μm are a couple of the galaxies approaching the detection limit of the instrument because of the combination of lower sensitivity at these wavelengths and a minimum in the spectral energy distribution as can be seen in Figure 2. In particular, the detection of these galaxies at 8.0 μm indicates more emission from hot dust and/or PAHs than might be expected for such low-luminosity and generally low-metallicity systems. Figure 3 shows the distribution of fluxes at 3.6 and 8.0 μm for the galaxies in the sample.

The galaxies have been selected to be low-luminosity systems with a luminosity limit of $M_B > -18.0$ – one galaxy that is at this limit within the errors ($M_B = -18.01$) is also included. After correcting for internal extinction using the ad hoc method developed by Melbourne and Salzer (2002) we have found that three additional objects are significantly higher luminosity galaxies. There are two additional galaxies for which the spectra are not of high enough quality to determine whether an extinction correction is appropriate. These are the two systems in Table 1 that do not have measured metallicities. We continue to include all nineteen galaxies in the sample and indicate which galaxies do not have a measured internal extinction correction and which galaxies do not have measured metallicities. We analyse the higher-luminosity galaxies separately since they are not actually part of the dwarf galaxy sample. The distributions of B, 3.6 μm, and 8.0 μm absolute magnitudes are shown in Figure 4. The black B-band histogram shows the uncorrected magnitudes while the shaded grey histogram shows the magnitudes corrected for internal extinction. The median magnitudes for the sample are M_{B0}=-17.67 (corrected for internal extinction), $M_{3.6}$= -20.68, and $M_{8.0}$=-22.87, shown in the figure with dashed lines.

As an objective prism survey, KISS detects galaxies based on the presence of emission lines rather than a broad-band flux limit. The emission-line detection makes this survey sensitive to more distant dwarf galaxies than a traditional flux-limited sample. The dwarf galaxies represented in this study have distances up to 295 h_{75}^{-1} Mpc and have a median distance of 115 h_{75}^{-1} Mpc. The distribution of velocities for the sample is shown in Figure 5. The dwarf sample is shown with the shaded histogram,

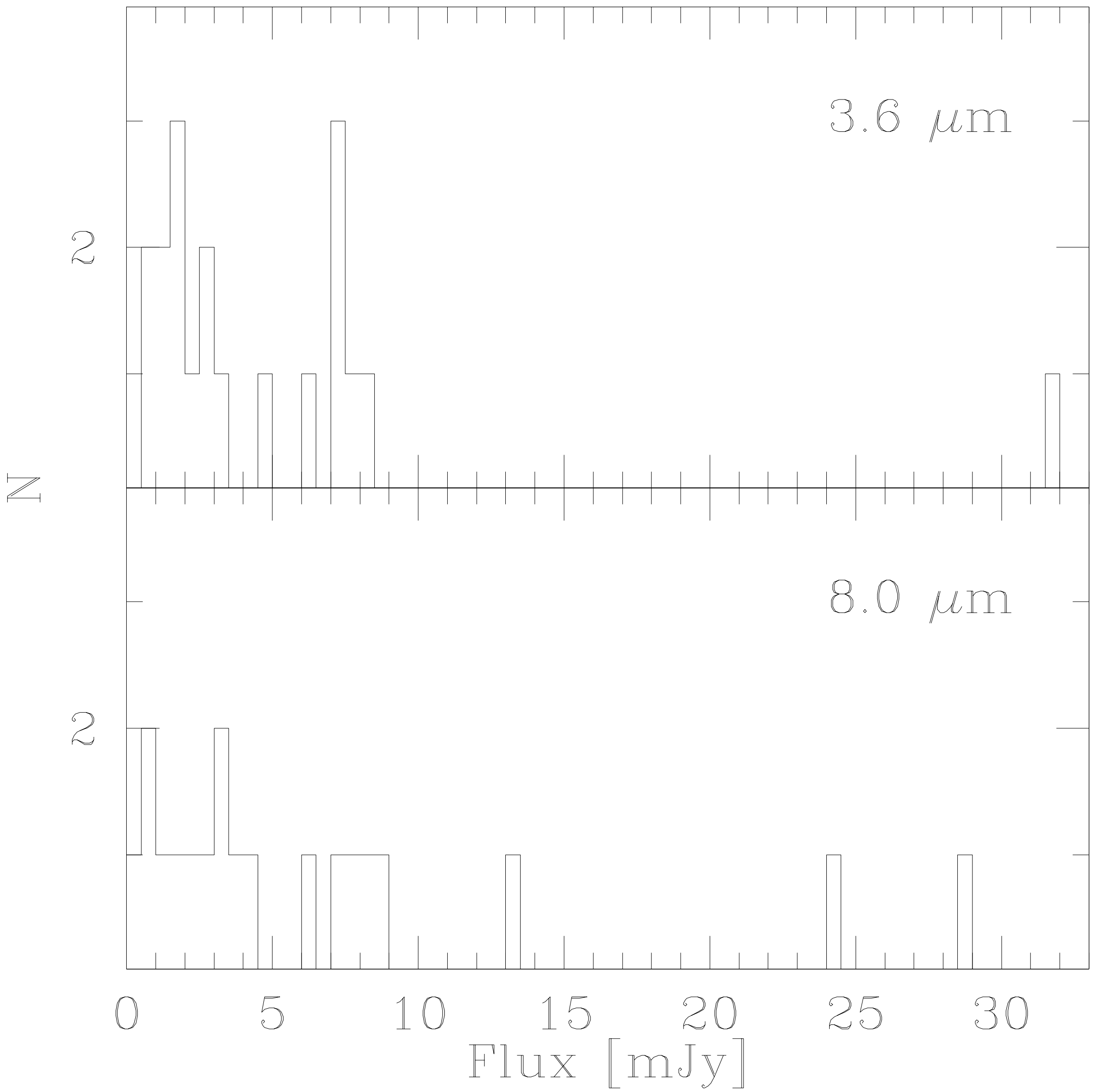

FIG. 3.— The distribution of fluxes (in mJy) at 3.6 and 8.0 μm for the sample galaxies.

the full sample with the open histogram. Despite the large distances of the galaxies and short exposure times for the Shallow Survey data, all systems were detected. The median absolute magnitudes in the Spitzer bands allow us to estimate the maximum distance at which these objects could be detected in some of the deeper Spitzer fields. In the Chandra Deep Field South and the Hubble Deep Field North (each is a 1° × 0.5° field) which have been observed for 500 seconds, a galaxy with an 8.0 μm magnitude equal to the median for the sample would be a 10σ detection at a distance of 492 h_{75}^{-1} Mpc. For a much smaller, but deeper survey like the Groth Strip (2°× 10′) which was observed for 3 hours at each pointing, these galaxies would be 10σ detections at 1060 h_{75}^{-1} Mpc ($z = 0.23$).

The KISS galaxies in this sample are star-forming systems and, therefore, tend to have blue optical colors. Figure 6 shows the relationship between the mid-infrared [3.6] − [8.0] color and the optical B-R color. The small grey dots represent all of the objects identified as galaxies in the Shallow Survey catalog (version 1.1). For these objects we use the cataloged magnitudes ("auto" aperture magnitudes determined using SExtractor (Bertin and Arnouts 1996)). As noted by Hogg et al. (2005), the majority of the Shallow Survey galaxies fall in two limited regions of color-space. The locus of points with [3.6] − [8.0] $\sim$ 0.5 contains mostly early-type systems while the group of galaxies with redder [3.6] − [8.0] colors are generally late-type systems. The outliers ($0 <$ B-R < 4 and [3.6] − [8.0] < -1) in this plot may be objects with poorly measured magnitudes because of the automated nature of the measurement or they may be objects with extreme colors. Nevertheless, the plot provides a good way to see where the KISS galaxies fall with respect to colors of the galaxies within the Shallow Survey field. The KISS galaxies are denoted by three different point types in this and all subsequent plots. We

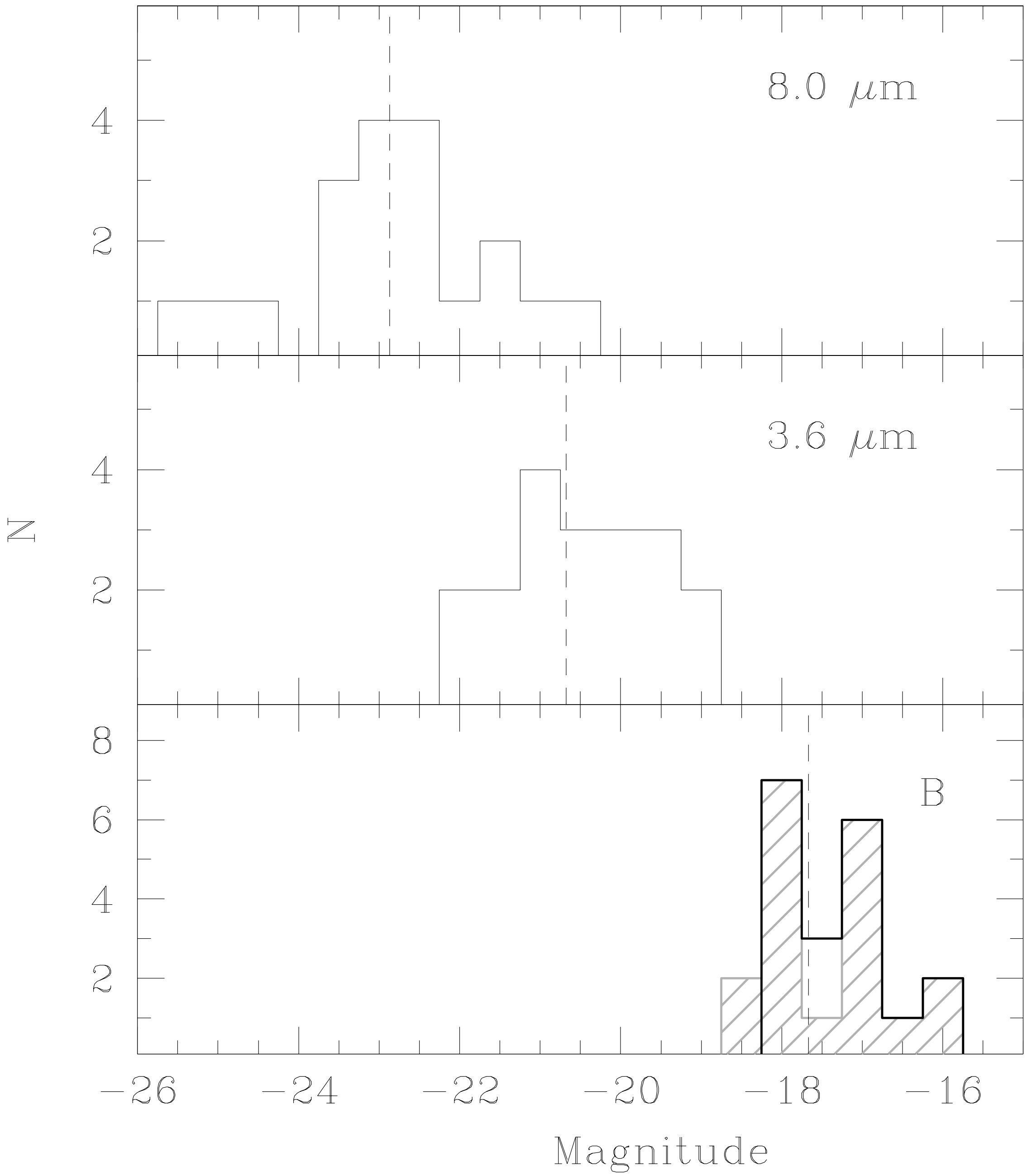

Fig. 4.— Histograms of galaxy absolute magnitudes in the B, 3.6 μm, and 8.0 μm bands. For the B-band histogram, the histogram under the black line indicates the distrution before correcting for internal extinction, while the shaded grey histogram is for the extinction-corrected distribution. The dashed lines indicate the median magnitudes of the sample in each band. Note that these galaxies have been selected to have $M_B >$ -18, but there are 3 galaxies that are brighter than that limit.

denote the four galaxies that turn out to be more luminous than $M_B = -18$ after the correction for internal extinction by $\times$'s. The two galaxies for which the spectra are not good enough to determine whether a correction for internal extinction should be applied (or to measure an abundance) are denoted by open circles. The rest of the galaxies are denoted by filled black circles. These objects have enough data to indicate that they are probably true dwarf galaxies by our luminosity criteria. The optical colors for the KISS galaxies in Figure 6 have not been corrected for extinction for consistency with the colors of the full galaxy sample. While the KISS galaxies are blue optically, they span the red end of the range of mid-infrared colors.

The mid-infrared colors of the KISS galaxies are only slightly correlated with the absolute 3.6 μm luminosities of the systems as shown in Figure 7. The figure indicates that the bluest galaxies in the mid-infrared are the lowest luminosity systems, but the colors have a spread of up to 2 magnitudes for any given 3.6 μm luminosity.

3.2. *Dust Properties*

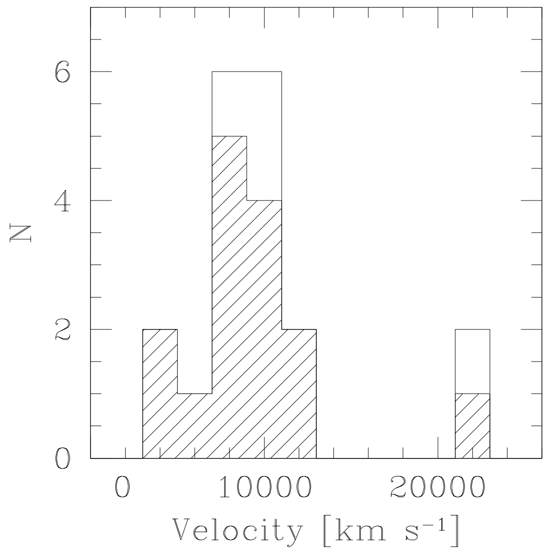

FIG. 5.— The distribution of velocities for the galaxies. The median distance at which the galaxies are detected is 115 h_{75}^{-1}Mpc for the dwarfs, galaxies with $M_B < -18.0$, shown with the shaded histogram and 120 h_{75}^{-1}Mpc for the full sample, which includes galaxies found to be brighter than $M_B = -18.0$ after correcting for extinction, shown with the open histogram.

Figure 6 and all of the subsequent figures showing the [3.6] − [8.0] colors for the KISS galaxies indicate that these systems span a wide range of mid-infrared colors. This range is an indication that some of the galaxies have very high dust-to-stars ratios while others do not, as illustrated in Figure 2. The high dust-to-stars ratios are evidence for strong emission from hot dust and/or PAHs, but without spectroscopy it is impossible to distinguish between a steep slope to the dust continuum and a PAH emission line. However, the evidence from the study of low-metallicity galaxies by Engelbracht et al. (2005) is that most low-metallicity systems have a deficit of PAH emission, but an excess of hot dust. This analysis is certainly consistent with the colors of these dwarf galaxies which also tend to be low-metallicity systems.

The reddening at Hβ ($c_{H\beta}$) provides a line-of-sight measurement of the optical extinction from the dust (Osterbrock 1989). Figure 8 shows the relationship between the [3.6] − [8.0] color and the $c_{H\beta}$ ratio. Two of the most luminous galaxies in the sample (brighter than the M_B=-18 cutoff after correction for extinction) have the highest $c_{H\beta}$ ratios and very red mid-infrared colors. However, for the rest of the galaxies in the sample, there is no correlation between the $c_{H\beta}$ ratios and the mid-infrared color. The amount of line-of-sight dust absorption implied by the $c_{H\beta}$ parameter is not a good predictor of the amount of mid-infrared dust emission present in these galaxies. The same result was found by Salzer & MacAlpine (1988) for the FIR emission in galaxies.

3.3. *Metallicity*

The KISS galaxies are low luminosity and mostly metal poor systems, making them potential analogs of the galactic building blocks at high redshift. We use the emission-line measurements from the follow-up spectroscopy to derive the [N II]/Hα and [O III]/Hβ ratios for the galaxies. These ratios are used to determine the galaxies' metallicity as described in Salzer et al. (2005b). Seventeen of the nineteen galaxies have measured line ratios and, therefore, calculated metallicities. The other two galaxies possess noisy spectra where some of the emission lines needed for deriving a metallicity estimate could not be measured.

While there is one super-solar metallicity source (KISS 2316), it has a luminosity that is brighter than the M_B=18 cutoff after it is corrected for extinction. All of the dwarf galaxies are significantly sub-solar ($[\log(O/H)+12]_\odot$ = 8.66, Asplund et al. 2004). The four most metal-rich systems are more luminous than $M_B = -18$. If one ignores these higher luminosity galaxies and considers only the dwarfs, then the median metallicity is 8.05 (0.25 $Z_\odot$) and the galaxies span the range from 0.15 to 0.51 $Z_\odot$ as shown in Figure 9. In this figure the shaded histogram shows the abundance distribution for the dwarfs while the open histogram shows the distribution for the full sample.

The correlation between luminosity and metallicity provides a probe of the relationship between the metallicity of a galaxy and either the stellar mass as measured by the B or 3.6 μm luminosity or the mid-infrared emission from dust as measured by the 8.0 μm luminosity. Figure 10 shows these correlations for the KISS sample. The B-band magnitudes have been corrected for extinction (for the 3 red, high $c_H\beta$ sources) – the galaxies for which the internal extinction correction is uncertain do not have measured abundances so they are not plotted. The fits to these relations include only the dwarf galaxies in the sample.

In addition to the correlation between the B-band and 3.6 μm luminosities and the metallicity, the 8.0μm luminosity is also correlated with metallicity. This result indicates that even in these low-metallicity systems which might not have PAHs, the hot dust and/or PAH emission is correlated with metallicity.

The slope of the luminosity-metallicity relationship shown in Figure 10 is very shallow in all three bands – -0.07 (8.0 μm), -0.16 (3.6 μm), and -0.16 (B-band). These slopes are in contrast with the slopes for a sample of KISS star-forming galaxies covering a large range in luminosity, $-22 < M_B < -12$, which have a steeper B-band slope of -0.28 (Salzer et al. 2005b, computed using the (Edmunds and Pagel 1984) metallicity calibration as was also done for the KISS galaxies presented here). However, the slope is consistent with those obtained for dwarf galaxy samples studied by Lee et al. (2004), Skillman et al. (1989) and Richer and McCall (1995) which have B-band slopes of -0.15 and by Shi et al. (2005) whose dwarf sample has a slope of -0.17. These data provide further evidence for the dwarf galaxy relation having a flatter slope than that exhibited by the more luminous systems. The interpretation of the extremely shallow slope at 8.0 μm will have to wait until we have a better understanding of the nature of this emission (e.g., the exact mixture of PAH and hot dust emission).

The *rms* scatter in metallicity around these fits is 0.17 (8.0 μm), 0.16 (3.6 μm), and 0.16 (B-band) respectively. If stellar mass and metallicity are correlated the scatter at 3.6μm should be tighter than in the B-band because

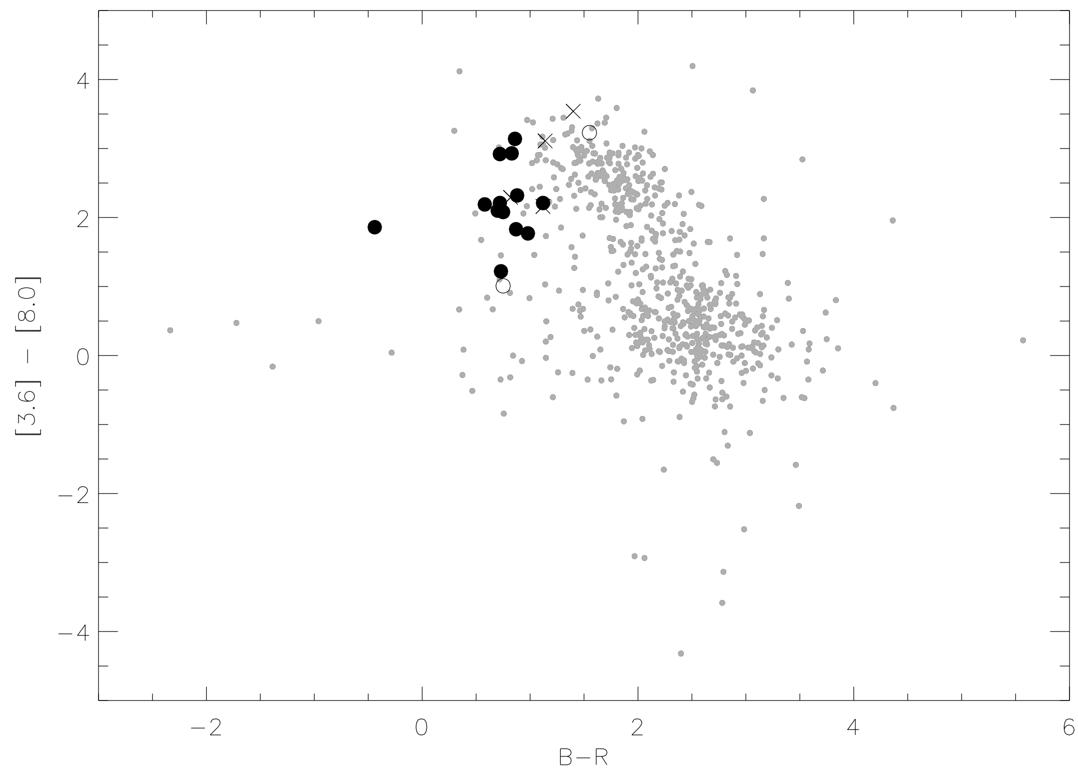

Fig. 6.— The mid-infrared versus optical colors for galaxies in the Shallow Survey (Eisenhardt et al. 2004, gray dots) and for KISS dwarf galaxies. The filled black circles show the true dwarfs in the KISS sample, the ×s are galaxies that are brighter than $M_B = -18$, and the open circles are the galaxies for which an internal extinction correction is not determined. No extinction correction has been applied to the optical colors of the KISS galaxies for comparison with the values measured for galaxies in the full Shallow Survey sample.

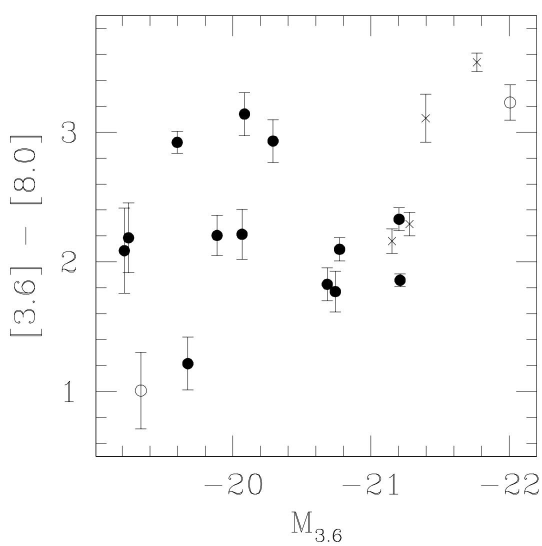

Fig. 7.— The mid-infrared color of the KISS galaxies as a function of the 3.6 μm luminosity. The ×s represent the galaxies brighter than M_B = -18, the open circles represent the galaxies for which no correction for internal extinction could be estimated.

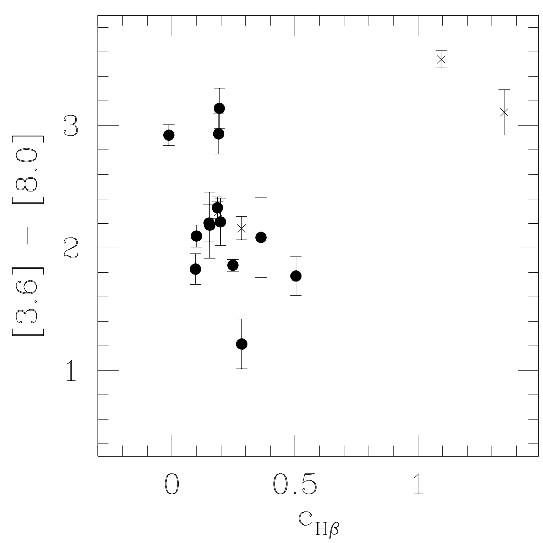

Fig. 8.— The relationship between the [3.6] − [8.0] color and the optical reddening at Hβ, $c_{H\beta}$. The filled circles are the true dwarfs, the ×s are galaxies that are brighter than $M_B = -18$.

extinction is less of a factor. We do not see any evidence for a lower scatter or a different slope at 3.6 μm.

Figure 11 shows the relationship between the mid-infrared color (dust-to-stars ratio) and the metallicity of the KISS galaxies. While the figure shows that the more metal-rich galaxies all have red mid-infrared colors, three of the galaxies with the reddest [3.6] − [8.0] are low-metallicity systems. Clearly metallicity is not the primary factor driving the dust-to-stars ratio in these

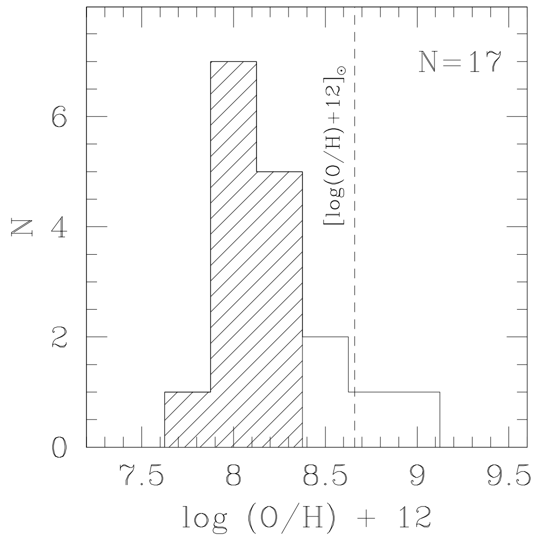

FIG. 9.— The distribution of log(O/H)+12 for the KISS dwarf galaxies. The dashed line indicates solar metallicity ([log(O/H)+12 = 8.66], Asplund et al. 2004). While there are a couple of solar metallicity sources, all of them are luminous objects. The shaded region shows the galaxies with M_B fainter than -18 all of which are significantly sub-solar with a median metallicity of 8.05 (0.25 $Z_\odot$).

galaxies, particularly for the low-luminosity systems.

3.4. *Star-Formation Rates*

The KISS dwarf galaxies are star-forming systems identified by the presence of optical emission lines. The distribution of star-formation rates in these galaxies can be seen in Figure 12. These star-formation rates have been derived from the Hα luminosity as in Kennicutt (1998), but the values have been corrected for the metallicity of the systems. For the galaxies for which the metallicity is not determined (2 systems), the standard Kennicutt (1998) conversion is used. The metallicity correction takes into account the difference between the number of Lyman continuum photons in solar metallicity models and models with lower metallicities that are closer in value to the observed abundances of our dwarf star-forming galaxies. The correction method is detailed in Lee et al. (2002). The radiation field in low metallicity systems is much harder so the inferred star-formation rate is somewhat lower at a given Hα luminosity compared to a metal-rich galaxy. Two of the three galaxies with high star-formation rates are luminous systems while the third is one of the galaxies with a noisy spectrum so it might also be a higher luminosity source. The star-formation rates for the dwarf galaxies are modest for low-luminosity systems – the rates are not as high as they are in some of the most strongly star-forming blue compact dwarf galaxies but they are still fairly strong for such low-luminosity dwarfs.

Figure 12 shows the relationship between mid-infrared color and SFR for the KISS galaxies. The galaxies without an internal extinction correction do not have a measured metallicity so the SFR determined from the standard Kennicutt (1998) conversion is probably an overestimate. While Figure 11 shows that some of the low-metallicity systems in this sample have red [3.6] − [8.0], Figure 12 shows that all of the red galaxies have high star-formation rates. The strength of the 8.0 μm dust emission is much more strongly correlated with the star-formation rate than it is with the metallicity of these systems.

4. DISCUSSION

We have presented the observations of 19 star-forming galaxies from the KISS survey observed with the IRAC camera on the Spitzer Space Telescope. Despite the small fraction of star-forming dwarf galaxies detected with IRAS (Salzer & MacAlpine 1988), we have detected all sample galaxies. Many are quite bright at mid-infrared wavelengths, as shown in Figures 3 and 4. In particular, the emission detected at 8.0 μm indicates a significant amount of dust resides in some of these systems.

One of the most striking features of the KISS sample in the mid-infrared is its diversity. This is a complete sample of low-luminosity galaxies that show evidence for star-formation through the presence of an Hα emission line. We find that the mid-infrared colors for some of the galaxies resemble those of dust-poor, low star-formation early-type galaxies while others have colors as red or redder than the late-type galaxy population (Pahre et al. 2004). The red colors are indicative of hot dust and/or PAH emission in these systems. The galaxies with bluer colors have low star formation rates and may also have a lower dust content or a lack of hot dust. If corruption of the 3.6 μm flux by hot dust is a problem it might result in blue colors like those seen for some of these dwarf galaxies. However, the shape of the SED shown in Figure 2 and the correlation between low star-formation rates and blue colors in these galaxies makes corruption of the 3.6 μm flux by hot dust an unlikely explanation.

Hogg et al. (2005) found that the low-luminosity galaxies in the overlap between the Sloan Digital Sky Survey and the Spitzer First Look Survey had significantly bluer mid-infrared colors than the higher luminosity systems with similar optical colors. The galaxies in the KISS sample also show a significant number of systems with blue optical and mid-infrared colors. However, we also note that in our sample and, in smaller numbers (possibly because they were not selecting star-forming dwarf galaxies in particular) in the Hogg et al. (2005) sample, the reddest low-luminosity galaxies are consistent with the reddest high luminosity systems with comparable optical colors. In the Hogg et al. (2005) sample the reddest high luminosity objects have [3.6] − [8.0] $\sim$ 3.9 (all comparisons here are converted to the Vega magnitude system) but most of the late-type galaxies have colors that are closer to [3.6] − [8.0] $\sim$ 2.8. The reddest low-luminosity galaxies in the Hogg et al. (2005) sample have [3.6] − [8.0] $\sim$ 2.7 while the reddest KISS galaxies have [3.6] − [8.0] $\sim$ 3.1.

Hogg et al. (2005) proposed that the deficit of red mid-infrared colors for low-luminosity galaxies in their sample could indicate that the supernova driven hot winds are driving dust and metals out the galaxies as happens to low-mass halos in the simulations of Mac Low and Ferrara (1999). The correlation between luminosity and metallicity in galaxies has also been used as a probe of the relationship between a galaxy's stellar population and the build-up of metals. In the KISS sample we find a significant number of low-luminosity galaxies with very red mid-infrared colors which clearly

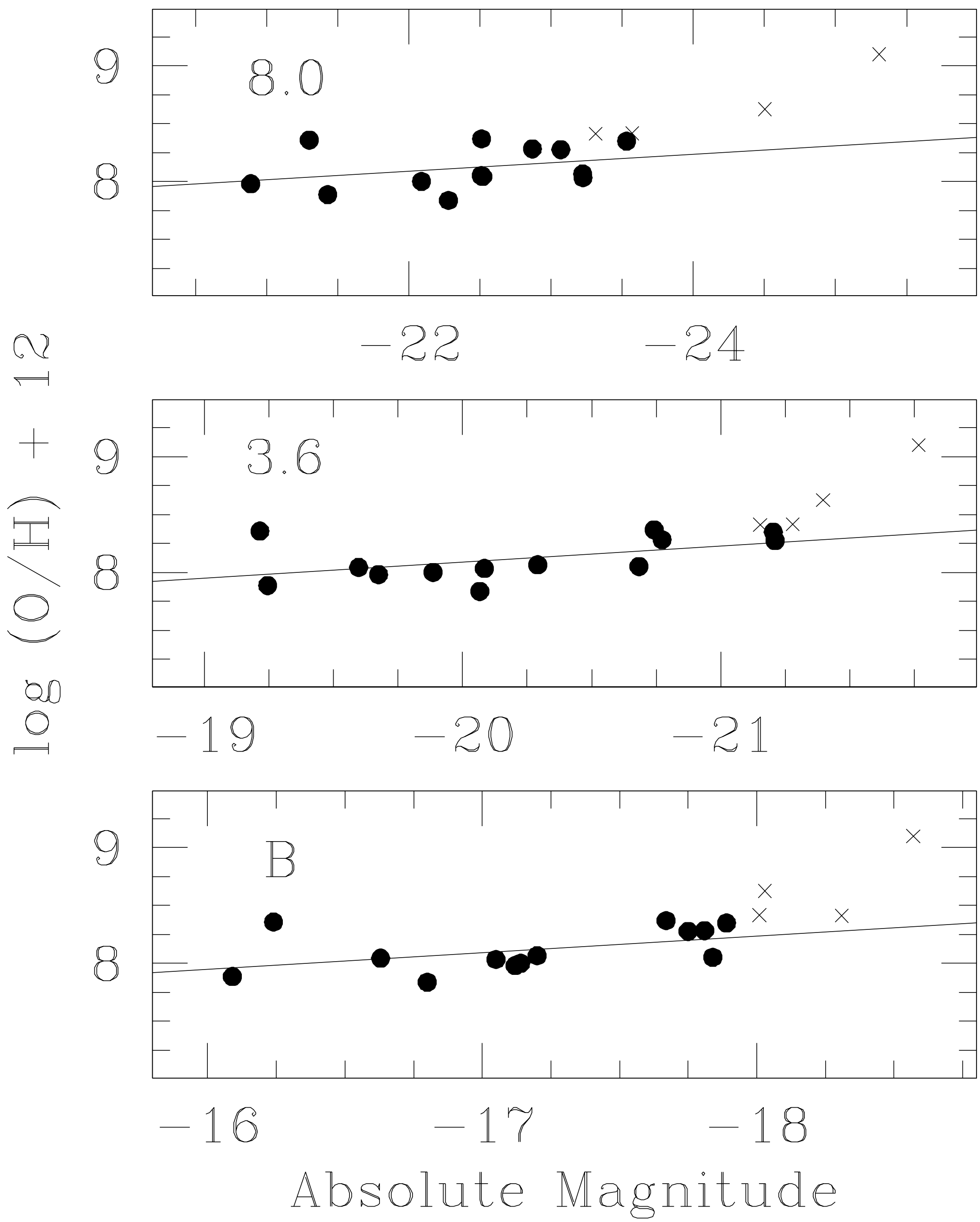

FIG. 10.— The relationship between metallicity and luminosity measured in the B, 3.6 μm, and 8.0 μm bands. The ×s indicate the galaxies brighter than $M_B = -18$ after correcting for internal extinction. The lines indicate linear least squares fits to the galaxies fainter than $M_B = -18$.

indicate the presence of hot dust and/or PAHs. This finding may indicate that the dust is not escaping from these galaxies as has been conjectured or that we are not probing the escaping dust. Instead we may be probing a region very close to the star formation where the temperatures and possibly the dust properties in these low-metallicity systems might be different from those of the general galaxy population. This latter possibility is would help explain the observation that 8.0 μm dust emission is better correlated with star-formation rate then it is with metallicity.

Figure 7 shows that some of the lowest mass galaxies, as indicated by their 3.6 μm luminosity, are also very blue and might be good candidates for dust expulsion

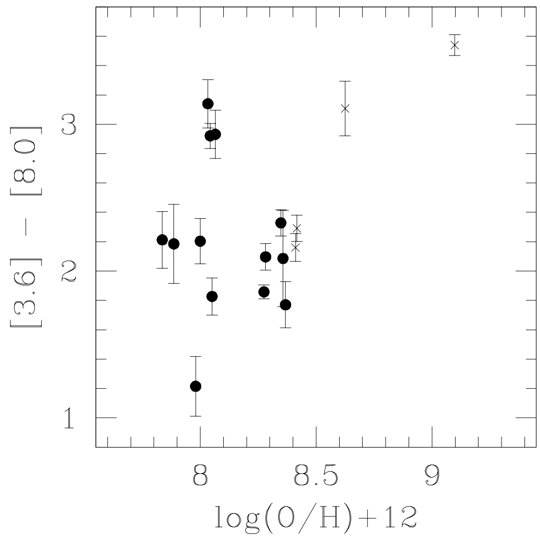

FIG. 11.— The relationship between the [3.6] − [8.0] μm color and metallicity. The ×s indicates galaxies that are brighter than $M_B = -18$.

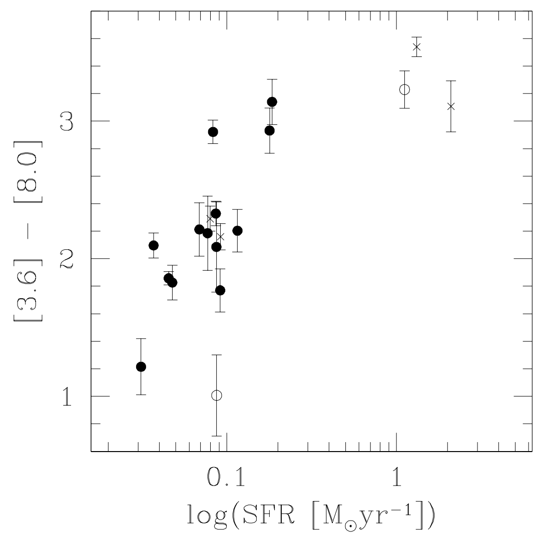

FIG. 12.— The relationship between the [3.6] − [8.0] μm color and the star-formation rate in these galaxies as measured from the Hα luminosity. The filled circles are the true dwarfs, the ×s are galaxies that are brighter than $M_B = -18$, and the open circles are the galaxies for which an internal extinction correction is not determined.

by the winds. These are the same galaxies in Figure 10 that are low luminosity at 3.6 μm and B-band and are also low metallicity, possibly further corroborating the notion that some of the metals and the dust is escaping. On the other hand, there are also low-mass galaxies that have red mid-infrared colors, indicating that they have been able to retain their dust, but are still low-metallicity systems. Clearly a measurement of the dynamical mass of these galaxies, rather than just a measurement of the stellar mass, is important for determining whether the galaxies with blue colors are the lowest mass halos. Alternatively, these galaxies with blue colors in the mid-infrared may just be producing less dust or be less efficient at heating it rather than losing it in winds since they have the lowest star-formation rates.

The correlation between B-band luminosity and metallicity shown in Figure 10 has been observed before and our results are completely consistent with the previous results for dwarf galaxies. It has been noted that one would expect to see this relation extended into the mid-infrared since the 3.6 μm emission is also tied to the stellar mass of the galaxy and that is indeed what this figure shows. The more surprising result is that we also see a correlation between the 8.0 μm luminosity and metallicity indicating that even in these low-metallicity systems, the emission from hot dust (or PAHs if they are present) is correlated with the metallicity of the system. It is unclear whether this result is due to dust grain size, temperature distribution in the star-forming regions, or some other physical property.

While we find that the 8.0 μm dust emission is correlated with star formation much more than it is with metallicity in the KISS galaxies (Figure 12), the connection between the hot dust/PAH emission seen at these mid-infrared wavelengths and the dust responsible for extinction at optical wavelengths is much less clear. For the 2 galaxies in our sample with very high values of $c_{H\beta}$ (greater than 1), the mid-infrared colors are very red indicating high dust-to-stars ratios. However, for galaxies with lower values of $c_{H\beta}$, there is no evidence for a correlation with the mid-infrared color. These results are consistent with IRAS observations of star-forming dwarf galaxies that showed no correlation between $c_{H\beta}$ and far infrared luminosity (Salzer & MacAlpine 1988; Kunth and Sevre 1985). While the mid-infrared emission measured in these star-forming dwarf galaxies indicates that these systems contain hot dust and/or PAHs, the amount of line-of-sight dust absorption implied by the $c_{H\beta}$ parameter is not a good predictor of the amount of mid-IR dust emission present as is also the case in the FIR (Salzer & MacAlpine 1988).

The mid-infrared observations of these star-forming dwarf galaxies have highlighted some surprising features of these systems which need to be investigated further. The spectral energy distributions from the optical through 24 μm (and in a few cases through 160 μm) in these galaxies will be presented in a forthcoming paper and will provide a much more detailed look at the properties of the stars and dust. In addition, it will be important to obtain systematic spectral observations of a sample of these dwarf galaxies to resolve the question of whether the mid-infrared emission is due to hot dust or the presence of a PAH feature at these wavelengths.

This work is based on observations made with the Spitzer Space Telescope, which is operated by the Jet Propulsion Laboratory, California Institute of Technology under NASA contract 1407. Support for this work was provided by NASA through a IRAC GTO award issued by JPL/Caltech under contract # 1256790. JLR acknowledges support from NSF grant AST-0302049. JJS gratefully acknowledges support for the KISS project from the NSF through grants AST 95-53020, AST 00-71114, and AST 03-07766. This work also made use of data products provided by the NOAO Deep Wide-Field Survey (Jannuzi and Dey 1999; Jannuzi et al. 2005; Dey et al. 2005), which is supported by the National Optical

Astronomy Observatory (NOAO). NOAO is operated by AURA, Inc., under a cooperative agreement with the National Science Foundation. Data products from the Two Micron All Sky Survey, which is a joint project of the University of Massachusetts and the Infrared Processing and Analysis Center/California Institute of Technology, funded by the National Aeronautics and Space Administration and the National Science Foundation were also used.

REFERENCES

Asplund, M., Grevesse, N., Sauval, A. J., Allende Prieto, C., and Kiselman, D.: 2004, *A&A* **417**, 751
Bertin, E. and Arnouts, S.: 1996, *A&AS* **117**, 393
Coleman, G. D., Wu, C.-C., and Weedman, D. W.: 1980, *ApJS* **43**, 393
Dey, A. et al.: 2005, *submitted*
Dwek, E., et al. 1998, *ApJ* **508**, 106
Edmunds, M. G. and Pagel, B. E. J.: 1984, *MNRAS* **211**, 507
Eisenhardt, P. R., et al. 2004, *ApJS* **154**, 48
Engelbracht, C. W., Gordon, K. D., Rieke, G. H., Werner, M. W., Dale, D. A., and Latter, W. B.: 2005, *ApJ* **628**, L29
Fazio, G. G., et al. 2004, *ApJS* **154**, 10
Ferrara, A. and Tolstoy, E.: 2000, *MNRAS* **313**, 291
Galliano, F., Madden, S. C., Jones, A. P., Wilson, C. D., and Bernard, J.-P.: 2005, *A&A* **434**, 867
Galliano, F., Madden, S. C., Jones, A. P., Wilson, C. D., Bernard, J.-P., and Le Peintre, F.: 2003, *A&A* **407**, 159
Gronwall, C., Salzer, J. J., Sarajedini, V. L., Jangren, A., Chomiuk, L., Moody, J. W., Frattare, L. M., and Boroson, T. A.: 2004, *AJ* **127**, 1943
Hogg, D. W., Tremonti, C. A., Blanton, M. R., Finkbeiner, D. P., Padmanabhan, N., Quintero, A. D., Schlegel, D. J., and Wherry, N.: 2005, *ApJ* **624**, 162
Houck, J. R., et al. 2004, *ApJS* **154**, 211
Izotov, Y. I., Lipovetsky, V. A., Chaffee, F. H., Foltz, C. B., Guseva, N. G., and Kniazev, A. Y.: 1997, *ApJ* **476**, 698
Jangren, A., Salzer, J. J., Sarajedini, V. L., Gronwall, C., Werk, J., Chomiuk, L. B., Moody, J. W., and Boroson, T. A.: 2005, *AJ* submitted (KR3)
Jannuzi, B. T. and Dey, A.: 1999, in *ASP Conf. Ser. 191: Photometric Redshifts and the Detection of High Redshift Galaxies*, pp 111–+
Jannuzi, R. T. et al. 2005, *submitted*
Kennicutt, R. C.: 1998, *ApJ* **498**, 541
Kravtsov, A. V., Gnedin, O. Y., and Klypin, A. A.: 2004, *ApJ* **609**, 482
Kunth, D. and Sevre, F.: 1985, in *Star-Forming Dwarf Galaxies and Related Objects*, pp 331–+
Lee, J. C., Salzer, J. J., Impey, C., Thuan, T. X., and Gronwall, C.: 2002, *AJ* **124**, 3088
Lee, J. C., Salzer, J. J., and Melbourne, J.: 2004, *ApJ* **616**, 752
Lu, N., et al. 2003, *ApJ* **588**, 199
Mac Low, M. and Ferrara, A.: 1999, *ApJ* **513**, 142
MacAlpine, G. M., Smith, S. B., and Lewis, D. W.: 1977, *ApJS* **34**, 95
Marengo, M. et al.: 2005, in preparation.
Markarian, B. E.: 1967, *Astrofizika* **3**, 55
Melbourne, J. and Salzer, J. J.: 2002, *AJ* **123**, 2302
Osterbrock, D. E.: 1989, *Astrophysics of Gaseous Nebulae and Active Galactic Nuclei*, University Science Books, Mill Valley, California
Pahre, M. A., Ashby, M. L. N., Fazio, G. G., and Willner, S. P.: 2004, *ApJS* **154**, 235
Plante, S. and Sauvage, M.: 2002, *AJ* **124**, 1995
Richer, M. G. and McCall, M. L.: 1995, *ApJ* **445**, 642
Roussel, H., Gil de Paz, A., Seibert, M., Helou, G., Madore, B. F., and Martin, C.: 2005, *ArXiv Astrophysics e-prints*
Salzer, J. J., et al. 2000, *AJ* **120**, 80
Salzer, J. J., et al. 2001, *AJ* **121**, 66
Salzer, J. J., et al. 2002, *AJ* **123**, 1292
Salzer, J. J., Jangren, A., Gronwall, C., Werk, J. K., Chomiuk, L. B., Caperton, K. A., and McKinstry, K.: 2005a, *AJ* submitted
Salzer, J. J., Lee, J. C., Melbourne, J., Hinz, J. L., Alonso-Herrero, A., and Jangren, A.: 2005b, *ApJ* **624**, 661
Salzer, J. J. and MacAlpine, G. M.: 1988, *AJ* **96**, 1192
Shi, F., Kong, X., Li, C., and Cheng, F. Z.: 2005, *A&A* **437**, 849
Silich, S. and Tenorio-Tagle, G.: 2001, *ApJ* **552**, 91
Skillman, E. D., Kennicutt, R. C., and Hodge, P. W.: 1989, *ApJ* **347**, 875
Smith, M. G., Aguirre, C., and Zemelman, M.: 1976, *ApJS* **32**, 217
Thuan, T. X., Sauvage, M., and Madden, S.: 1999, *ApJ* **516**, 783
Wasilewski, A. J.: 1983, *ApJ* **272**, 68
Werner, M. W., et al. 2004, *ApJS* **154**, 1
Zamorano, J., Rego, M., Gallego, J. G., Vitores, A. G., Gonzalez-Riestra, R., and Rodriguez-Caderot, G.: 1994, *ApJS* **95**, 387

TABLE 1
KITT PEAK INTERNATIONAL SPECTROSCOPIC SURVEY DATA

KISS#	Field	ID	RA J2000	Dec J2000	Vel. km s^{-1}	B	M_B	M_{B0} [1]	$(B-V)_0$ [2]	$c_{H\beta}$ [3]	$EW_{H\alpha}$ Å	log $L_{H\alpha}$ ergs s^{-1}	[NII]/Hα	[OIII]/Hβ	Abund. [4]	SFR [5] $M_\odot$ yr^{-1}
2292	H1426	8731	14:25:09.2	35:25:15.9	8659	17.62	-17.80	-18.31	0.66	0.283	38.4	40.39	-0.756	0.398	8.411	0.09
2300	G1426	6944	14:26:08.9	33:54:19.8	10271	19.70	-16.09	-16.09	0.50	0.154	301.6	40.52	-1.566	0.676	7.886	0.08
2302	H1426	5703	14:26:17.5	35:21:35.5	8342	18.18	-17.16	-17.16	0.42	...	25.1	40.04	...	...	...	0.09
2309	G1426	4670	14:26:53.6	34:04:14.5	7231	17.89	-17.12	-17.12	0.43	0.284	81.8	40.09	-1.402	0.653	7.980	0.03
2316	G1426	1167	14:28:14.9	33:30:25.7	10685	18.51	-17.38	-18.57	0.81	1.094	32.2	41.01	-0.475	-0.662	9.098	1.32
2318	H1426	299	14:28:24.6	35:10:21.5	22163	19.66	-17.88	-17.88	0.95	...	22.5	41.15	...	...	...	1.12
2322	G1430	9529	14:29:09.6	32:51:26.7	8574	17.53	-17.84	-17.84	0.53	0.096	73.2	40.24	-1.289	0.415	8.051	0.05
2326	G1430	7761	14:29:32.7	33:30:40.3	7935	18.07	-17.14	-17.14	0.51	0.151	189.8	40.65	-1.370	0.662	8.000	0.11
2338	H1430	4786	14:30:27.9	35:32:07.2	11689	18.89	-17.20	-17.20	0.77	0.190	258.7	40.81	-1.266	0.747	8.065	0.18
2344	H1430	3113	14:31:03.6	35:31:14.8	4166	16.06	-17.75	-17.75	0.44	0.248	217.2	40.12	-1.041	0.468	8.275	0.04
2346	G1430	3224	14:31:14.4	33:19:13.2	10819	19.09	-16.80	-16.80	0.67	0.197	122.8	40.49	-1.661	0.800	7.836	0.07
2349	H1430	3139	14:31:20.0	34:38:03.8	4396	17.30	-16.63	-16.63	0.52	-0.012	396.4	40.48	-1.300	0.665	8.043	0.08
2357	G1430	1974	14:31:39.2	33:26:32.3	10759	18.21	-17.67	-17.67	0.58	0.504	27.4	40.40	-0.808	0.461	8.368	0.09
2359	H1430	1039	14:31:49.3	35:28:40.0	22512	20.02	-17.55	-18.03	0.64	1.350	76.7	41.66	-0.452	0.161	8.625	2.09
2368	G1430	376	14:32:18.9	33:02:53.7	10972	18.88	-17.05	-17.05	0.76	0.193	245.4	40.84	-1.316	0.818	8.033	0.18
2382	H1434	5378	14:34:08.0	34:19:34.4	6813	17.07	-17.81	-17.81	0.35	0.100	33.4	40.03	-1.049	0.440	8.282	0.04
2398	H1437	8675	14:36:33.1	34:58:04.4	9006	17.50	-18.01	-18.01	0.46	0.187	35.8	40.33	-0.764	0.368	8.417	0.08
2403	G1437	5761	14:37:42.6	33:36:26.7	12047	19.91	-16.24	-16.24	0.36	0.362	103.8	40.38	-0.798	0.506	8.357	0.09
2406	H1437	3649	14:38:27.8	35:08:59.0	8641	17.51	-17.89	-17.89	0.49	0.185	19.4	40.38	-0.915	0.394	8.348	0.09

[1] B-band absolute magnitude corrected for internal extinction using the ad hoc method from Melbourne and Salzer (2002) (This correction is only applied to the three galaxies in the sample that are optically red and have a high $c_{H\beta}$. For all other galaxies $M_{B0} = M_B$.)

[2] B-V color corrected for Galactic absorption

[3] decimal reddening coefficient

[4] log (O/H) + 12, which is a measure of metallicity. For details of the calculation see Melbourne and Salzer (2002) and Salzer et al. (2005b).

[5] star-formation rate calculated from the Hα luminosity using the prescription of Kennicutt (1998) and then corrected for the effect of metallicity when an abundance measurement is available using the prescription of Lee et al. (2002). Two of the galaxies in the sample do not have measured abundances because the lines in these spectra are not high enough signal-to-noise to determine robust values.

TABLE 2
2MASS and NOAO Wide Deep Survey Photometry

KISS#	Field	ID	J_{2MASS}	H_{2MASS}	K_{2MASS}	B_{NDWFS}	R_{NDWFS}	I_{NDWFS}	K_{NDWFS}
2292	H1426	8731	···	···	···	17.67	16.50	16.03	14.55
2300	G1426	6944	···	···	···	19.76	19.12	18.81	17.53
2302	H1426	5703	···	···	···	18.20	17.43	17.07	14.89
2309	G1426	4670	···	···	···	17.93	17.16	16.73	15.75
2316	G1426	1167	16.0	15.2	14.8	18.50	17.11	16.57	···
2318	H1426	299	···	···	···	19.58	18.11	17.46	15.77
2322	G1430	9529	···	···	···	17.56	16.66	16.21	···
2326	G1430	7761	···	···	···	18.03	17.35	17.06	···
2338	H1430	4786	···	···	···	18.94	18.06	17.73	16.01
2344	H1430	3113	···	···	···	17.14	16.50	16.22	15.22
2346	G1430	3224	···	···	···	19.07	17.97	17.30	···
2349	H1430	3139	16.3	16.2	15.5	17.33	16.58	16.32	14.90
2357	G1430	1974	···	···	···	18.21	17.23	16.85	···
2359	H1430	1039	···	···	···	20.07	18.88	18.38	16.50
2368	G1430	376	···	···	···	18.87	18.02	17.72	···
2382	H1434	5378	16.4	15.0	15.5	17.11	16.37	15.99	14.51
2398	H1437	8675	···	···	···	17.60	16.68	16.26	14.82
2403	G1437	5761	···	···	···	19.99	19.16	18.81	···
2406	H1437	3649	16.0	15.4	15.2	17.57	16.63	16.20	···

TABLE 3
Spitzer IRAC Photometry

KISS#	Field	ID	$R_{3.6}$ [″] [1]	Ellip. [2]	[3.6]	$\sigma_{3.6}$	[4.5]	$\sigma_{4.5}$	[5.8]	$\sigma_{5.8}$	[8.0]	$\sigma_{8.0}$
2292	H1426	8731	12	0.11	14.31	0.07	14.29	0.09	13.53	0.17	12.15	0.07
2300	G1426	6944	10	0.32	16.59	0.19	16.32	0.24	15.96	0.51	14.40	0.19
2302	H1426	5703	14	0.32	16.05	0.15	16.03	0.21	15.81	0.47	15.04	0.25
2309	G1426	4670	12	0.16	15.40	0.11	15.43	0.16	14.92	0.32	14.18	0.17
2316	G1426	1167	14	0.07	14.15	0.06	14.09	0.08	12.61	0.11	10.61	0.03
2318	H1426	299	14	0.35	15.50	0.11	15.31	0.15	14.68	0.28	12.27	0.07
2322	G1430	9529	20	0.22	14.76	0.08	14.68	0.11	14.31	0.24	12.93	0.10
2326	G1430	7761	14	0.19	15.39	0.11	15.33	0.15	14.56	0.27	13.18	0.11
2338	H1430	4786	14	0.18	15.82	0.13	15.49	0.16	14.60	0.27	12.89	0.09
2344	H1430	3113	70	0.70	12.66	0.03	12.53	0.04	11.56	0.07	10.80	0.04
2346	G1430	3224	12	0.08	15.88	0.14	15.80	0.19	15.25	0.37	13.67	0.14
2349	H1430	3139	20	0.32	14.39	0.07	14.10	0.09	12.94	0.13	11.47	0.05
2357	G1430	1974	20	0.57	15.19	0.10	15.01	0.13	14.89	0.31	13.42	0.12
2359	H1430	1039	12	0.05	16.14	0.16	15.96	0.20	15.69	0.45	13.03	0.10
2368	G1430	376	14	0.37	15.89	0.14	15.45	0.16	14.57	0.27	12.75	0.09
2382	H1434	5378	20	0.37	14.17	0.06	14.16	0.09	13.47	0.16	12.07	0.06
2398	H1437	8675	30	0.44	14.27	0.07	14.17	0.09	13.39	0.16	11.98	0.06
2403	G1437	5761	14	0.35	16.96	0.23	16.78	0.29	15.81	0.47	14.88	0.23
2406	H1437	3649	20	0.14	14.25	0.06	14.26	0.09	13.40	0.16	11.93	0.06

[1]The semi-major axis of the aperture in which the flux was measured
[2]The ellipticity of the fit aperture